Optical, x-ray, and band-structure studies of iodine at pressures of several megabars

Robin Reichlin, Andrew K. McMahan, Marvin Ross, and Sue Martin
Lawrence Livermore National Laboratory, University of California, Livermore, California 94550

Jingzhu Hu, Russell J. Hemley, Ho-kwang Mao, and Yan Wu
Geophysical Laboratory and Center for High-Pressure Research, Carnegie Institution of Washington, 5251 Broad Branch Road, NW, Washington, D.C. 20015

(Received 10 September 1993)

Optical-reflectivity and x-ray-diffraction techniques have been used to determine the electronic properties and structure of iodine to 181 and 276 GPa, respectively, in the diamond-anvil cell. X-ray measurements were performed by energy dispersive diffraction with synchrotron radiation. Monatomic metallic iodine transforms to an fcc structure at 53 GPa that remains stable to the maximum pressure. At 276 GPa, the volume compression V/V_0 is 0.324. Reflectivity data are consistent with a strong metallic character in iodine from 19 to 181 GPa. The linear muffin-tin orbital method has been used to calculate the equation of state to 500 GPa and to model the reflectivity of iodine at high pressures.

INTRODUCTION

It is now recognized that compression of solids to megabar pressures can produce major changes in their electronic structure and bonding properties, which in turn may drive structural phase transformations and induce insulator-metal transitions.[1] Filled-shell insulators, such as the rare-gas solid Xe and the ionic salt CsI, provide clear examples of these effects.[2–5] Diatomic molecular solids offer other examples, which are further complicated by the eventual pressure-induced dissociation of the molecules. The search for structural transformations, the insulator-metal transition, and dissociation in the case of solid hydrogen is currently the subject of intense research.[6] The solid halogens, which also form diatomic molecular solids at low pressure, provide another example of these phenomena. Of these materials, solid iodine has been of particular interest in view of its insulator-metal transition at 16 GPa,[7–9] and well-documented structural evolution which includes nonmolecular, monatomic metallic phases at higher pressures.[10–16] In the present study, we examine the behavior of this system at pressures well into the megabar range (> 100 GPa) by the use of optical and x-ray-diffraction techniques, as well as theoretical electronic-structure calculations.

The insulator-metal transition in iodine has been the subject of study for a number of years. At ambient conditions solid iodine is a diatomic molecular insulator with a base-centered orthorhombic crystal structure. Electrical-resistivity measurements indicate that iodine undergoes a continuous transition to the metallic state at around 16 GPa.[7–9] X-ray-diffraction data suggest that the molecular phase dissociates at 21 GPa and room temperature to a monatomic phase.[13,14] The molecular dissociation is a first-order transition with a volume change of 4%. Syassen *et al.*[17] found that the infrared reflectivity of iodine increased dramatically at the dissociation pressure, which they interpreted to be Drude-like behavior associated with increasing carrier density. They did not find any evidence of metallic character in the molecular-metallic phase based on reflectivity data.

There have also been numerous x-ray-diffraction studies of iodine at high pressure.[10–16] Three of these have examined the rearrangement of I_2 molecules with increasing pressure as the dissociation transition is approached from below.[10–12] The molecular dissociation at 21 GPa is to a body-centered orthorhombic (bco) phase,[13,14] which continuously approaches a body-centered tetragonal (bct) structure with increasing pressure, reaching that symmetry at 43 GPa in what appears to be a second-order transition.[15] Similarly, the c/a ratio of the bct phase continuously approaches that of a face-centered cubic (fcc) structure with increasing pressure; however, at 55 GPa, iodine undergoes a first-order transition to an fcc phase with a 1.8% volume change.[16] This fcc phase remains stable to 64 GPa, the highest pressure previously investigated in iodine.[16]

Pasternak *et al.*[18–20] have conducted Mössbauer (4 K) and Raman studies (300 K) of iodine to 30 GPa. They contend that their work, and an earlier Raman study by Shimomura *et al.*,[21] suggest that the structural phase transition at 21 GPa may not involve molecular dissociation of iodine. Fujihisa *et al.*,[22] however, have recently conducted x-ray-diffraction experiments at low temperatures and report molecular dissociation of iodine at 21 GPa and 35 K, casting doubt on the original interpretation of the Mössbauer data. The discrepancies between the Mössbauer and Raman studies on the one hand, and the x-ray and optical measurements on the other, have yet to be fully resolved at the 21-GPa phase boundary. However, the molecular dissociation of iodine at 21 GPa appears to be the most likely interpretation. The assignment of a monatomic fcc structure at 55 GPa is unquestioned. Nevertheless, it is of interest to examine the stability of the fcc phase to higher pressure, as theoretical calculations have shown a tendency for fcc-to-hcp transitions to occur at high pressure at least for filled-shell sys-

tems,[23] in agreement with the observed behavior of Xe (Refs. 2,3) and CsI (Ref. 5) at megabar pressures.

Previous theoretical work on iodine at high pressure includes a comparison of calculated total-energy results for an assumed fcc phase of iodine with shock-compression data, which suggested conversion to something like the monatomic state at pressures in the vicinity of the metallization transition,[24] in agreement with the subsequent x-ray results.[13,14] Other calculations have focused on the specific changes in electronic structure which bring about the insulator-metal transition,[25,26] and on the nature of hole conductivity in the monatomic phases at higher pressure.[27]

In the present paper, we report the results of x-ray-diffraction and optical-reflectivity measurements on monatomic-metallic iodine, taken up to pressures of 276 and 181 GPa, respectively, using the diamond-anvil cell. This work therefore considerably extends the pressure range over which iodine has been investigated, beyond the 64 and 30 GPa pressures attained in previous x-ray[16] and optical[17] experiments, respectively. We have found no evidence of further phase transitions above 55 GPa. Linear muffin-tin orbital calculations have also been used to obtain the pressure-volume curve for fcc iodine, in order to compare with the present x-ray-determined equation of state, and also to provide insight used to model the reflectivity of iodine at high pressures.

EXPERIMENTAL PROCEDURES

Iodine samples of 98.8% purity were loaded at room pressure and temperature into three megabar-type diamond-anvil cells. The type-Ia diamond anvils were double beveled in all of the experiments. In the first experiment, the anvils had a 70-μm-diameter central flat, 300-μm-diameter total culet, and 6° and 3° bevel angles (from center to edge). The second and third samples (I9 and I13) were confined in anvils with 50-μm-diameter central flat, 300-μm-diameter total culet, 7° and 10° bevel angles. Maximum pressures achieved were 142, 181, and 276 GPa, respectively. The sample chambers were formed by drilling a 30-μm-diameter hole in a 0.25-mm-thick rhenium gasket preindented to 30 GPa. Iodine was loaded with gold-coated instruments in a glove box under argon atmosphere to discourage reaction with water and other materials. An approximately 10×30 μm^2 piece of platinum foil was loaded into the chamber (on the piston diamond) and a small grain of solid iodine was placed on top of the platinum. A small amount of ruby dust (particles approximately 1 μm diameter) was placed on the cylinder diamond and the cell was closed and pressurized. The final sample chambers were approximately 30 μm in diameter. The diamond-sample interface used to measure optical properties contained only iodine and a small amount of ruby. The platinum foil was observed only at the other interface.

Single-beam reflectivity measurements were made in the energy range 0.5–4.0 eV. The infrared region of each spectrum (0.5–2.0 eV) was collected using techniques described elsewhere.[4] The visible region (1.3–4.0 eV) was measured using the same collection optics (without repositioning the sample) as above, but with a xenon arc source and a $\frac{3}{4}$-m spectrometer with 1800-groove/mm holographic grating and 310-μm slits. Signals were collected using a cooled GaAs photomultiplier tube.

Reflectivities were measured on the same 25-μm diameter sample area in each spectral region. Reflectivity was measured at the diamond-sample interface and was corrected to the reflectivity of the diamond-air interface over the same spectral region. Reference spectra at the diamond-air interface were collected immediately before and after each sample spectrum to minimize the effects of variations in source intensity. Iodine spectra were corrected for reflections at the diamond-air interface and for absorption in the diamonds.[28]

X-ray-diffraction measurements were made at the National Synchrotron Light Source, Brookhaven National Laboratory. The measurements were carried out using energy-dispersive x-ray-diffraction techniques.[2,5,29] The first set of x-ray measurements were carried out on the bending magnet beamline X7A, operating at 2.5 GeV and 100–200 mA. The incident x-ray beam from the synchrotron was collimated to a width$\times$height of 30×80 μm^2. The diffracted x-ray beam was collected with a Ge detector at approximately 18°-2θ scattering angle, which was calibrated with CeO_2 powder at ambient pressure. The second set of experiments were performed using the superconducting wiggler beamline (X17C) operating at 100–200 mA with a magnetic field of 4.6 T. The incident beam was collimated by 10×10 μm^2 slits located as close as possible to the sample (25 mm) to reduce the effect of the x-ray divergence and pressure gradients in the sample. The diffracted beam was collected at 15°-2θ scattering angle, and the angle was calibrated by using diffraction pattern of gold foil at ambient pressure. Data were also collected at lower 2θ angles (13° and 8°) to look for new reflections in the low-energy region. Data collection times ranged from 15 to 60 min, with higher acquisition times used at the higher pressures.

Sample pressures were measured in the diamond-anvil cell *in situ* using the ruby-fluorescence technique in the reflectivity experiments. In the case of ruby-fluorescence determinations, pressure was measured on numerous 1–2-μm ruby chips dispersed throughout the sample chamber. Excitation of the fluorescence was made with the 457.9-nm line of an argon-ion laser focused to a 5-μm diameter. Pressure variations within the sample chamber were less than 2 GPa up to 104 GPa. Calibrations were based on the quasihydrostatic ruby scale of Mao and coworkers.[30] Pressures were measured using platinium as internal standard for the x-ray-diffraction experiments. Lattice parameters of Pt were determined from the 111, 200, 220, 311, and 222 diffraction peaks. Pressures were then determined from the equation of state of Holmes *et al.*[31]

X-RAY DIFFRACTION RESULTS

In the first set of experiments, diffraction and optical data were collected from two samples to peak pressures of 142 and 181 GPa. X-ray-diffraction data were collected in the second set of measurements to maximum pres-

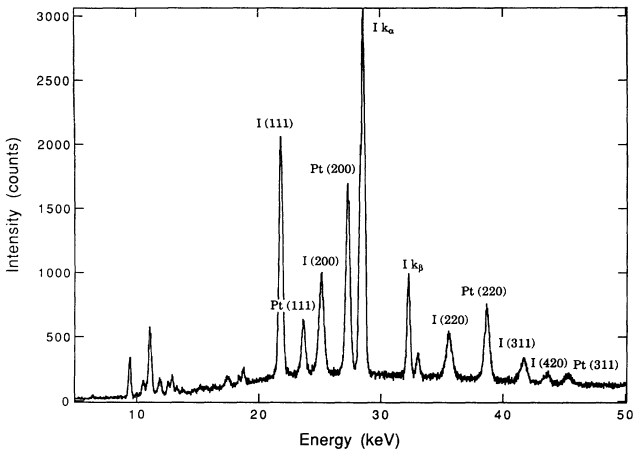

FIG. 1. The energy-dispersive x-ray-diffraction pattern of iodine with Pt as an internal pressure standard at pressure $P=266(3)$ GPa and room temperature. The diffraction angle was $2\theta=15.002°$.

sures of 276 GPa. At most pressures, five reflections of the fcc phase of iodine were obtained (i.e., 111, 200, 220, 311, and 222 diffraction peaks). Figure 1 shows the energy-dispersive x-ray-diffraction pattern with Pt as internal pressure standard at 266(3) GPa. The pressure dependence of d spacings of the fcc phase are shown in Fig. 2. No new diffraction peaks, indicative of a new high-pressure phase, were found to the maximum pressure reached (276 GPa).

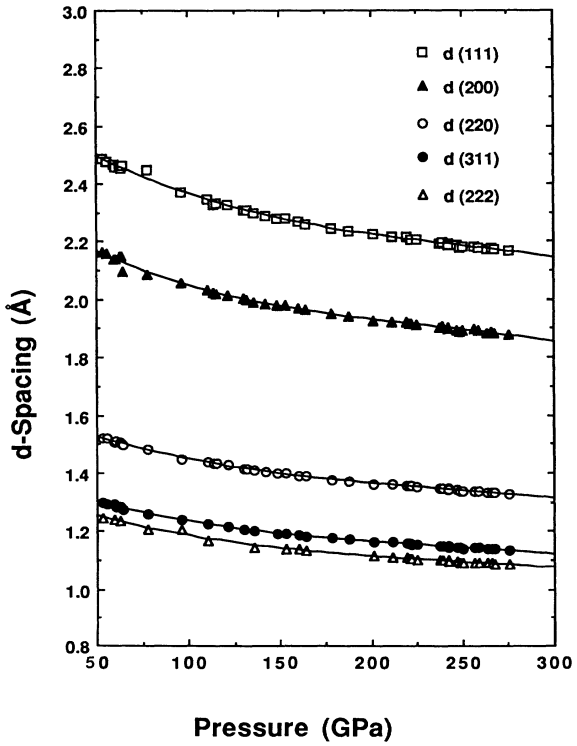

FIG. 2. Pressure dependence of the interplanar spacings for the fcc phase of iodine. The solid lines are the third-order polynomial equation fit to the experimental data.

The pressure-volume points for the fcc phase of iodine obtained from our x-ray measurements are listed in Table I. The data are plotted in Fig. 3, along with previous results for the fcc phase by Fujii *et al.*[16] and for other low-pressure phases by Fujii *et al.*[15] and by Takemura and co-workers.[13,14] The present results differ somewhat from those of Fujii *et al.*[16] The origin of this discrepancy is not understood but may be associated with the use of different pressure standards (ruby fluorescence versus Pt x ray) which could cause differences if pressure gradients are significant. In this regard, we emphasize that the

TABLE I. Pressure-volume data for the fcc phase of iodine. Measurements made at X17C superconducting wiggler beam line, except where noted.

Pressure (GPa)	Volume (Å^3/atom)
53.1(2.1)	19.91(81)
55.1(3.4)	19.82(65)
59.4(1.5)	19.45(47)
60.3(1.3)	19.39(87)
61.0(3.6)	19.26(35)
62.5(2.3)	19.26(01)
63.2(1.1)	19.16(01)
77.8(1.8)	18.24(08)
95.9(2.8)	17.31(08)
110(2)	16.74(08)
113(3)[a]	16.56(09)
115(3)[a]	16.55(06)
121(1)	16.35(01)
130(2)	16.03(06)
132(3)[a]	15.98(01)
135(2)	15.80(06)
142(3)[a]	15.68(05)
148(3)	15.49(08)
152(1)	15.44(05)
160(1)	15.22(05)
164(3)	15.09(05)
178(2)	14.80(05)
187(2)	14.58(03)
201(2)	14.33(01)
211(4)	14.19(06)
219(3)	14.17(04)
221(6)	14.07(04)
222(4)	14.02(03)
225(3)	13.39(03)
237(2)	13.76(03)
239(4)	13.82(04)
242(4)	13.74(03)
242(1)	13.69(02)
247(2)	13.59(01)
248(2)	13.48(07)
250(3)	13.51(03)
250(3)	13.53(02)
257(4)	13.54(06)
259(6)	13.51(07)
263(2)	13.38(03)
266(3)	13.43(04)
267(4)	13.36(03)
276(3)	13.25(04)

[a]Measured at X7A bending magnet beam line.

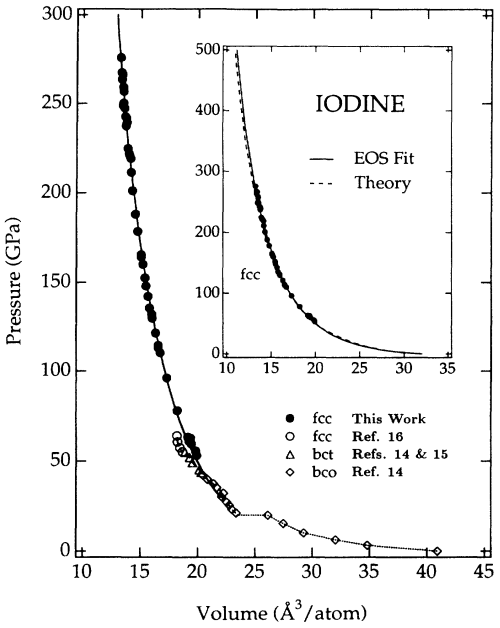

FIG. 3. Measured pressure-volume relations for iodine, including the present data for the fcc phase and previous work at lower pressures by Fujii *et al.* (Refs. 15 and 16) and Takemura and co-workers (Refs. 13 and 14). The inset compares the measured pressure-volume relation for fcc iodine (data points) to the LMTO theoretical result (dashed curve), and the Vinet fit to the experimental data (solid curve). Parameters used in the fit are $V_{0,\mathrm{fcc}}=31.25(\pm 0.07)$ Å^3/atom, $K_0=30.38(\pm 0.13)$ GPa, and $K_0'=6.13(\pm 0.01)$.

pressures were determined in this study from diffraction of the Pt at the same point in the sample where the iodine diffraction was measured. We also note that the phase transition pressure occurs at slightly lower pressure in our study (53 versus 55 GPa reported previously).

The solid line is an equation of state fit to the P-V data using the phenomenological relation proposed by Vinet *et al.*,[32]

$$P=3K_0\frac{1-x}{x^2}\exp[1.5(K_0'-1)(1-x)]\ ,$$

where $x=(V/V_{0,a})^{1/3}$, and $V_{0,a}$ is the zero-pressure volume of phase a, K_0 is the bulk modulus, and K_0' is the pressure derivative of the bulk modulus, each evaluated at zero pressure. Least-squares analysis yields best-fit parameters of $V_{0,\mathrm{fcc}}=31.25(\pm 0.07)$ Å^3/atom, $K_0=30.38(\pm 0.13)$ GPa, and $K_0'=6.13(\pm 0.01)$. The standard deviation in pressure is ± 3.3 GPa.

BAND-STRUCTURE CALCULATIONS

In order to make comparison with the present equation-of-state measurements, and to provide some insight into the reflectivity data to be presented shortly, we have carried out linear muffin-tin orbital (LMTO) calculations of the zero-temperature pressure-volume relation and of the joint density of states for fcc iodine as a function of volume. The LMTO method has been described in detail elsewhere.[33,34] The present calculations were scalar relativistic, employed the von Barth–Hedin exchange-correlation potential,[35] and included both the combined correction[33,34] and the Ewald[36] corrections beyond the atomic-sphere approximation.[33,34] The 5*spd* valence states were represented using *s-f* angular momentum components, and sampled with 89 points per irreducible wedge in the self-consistent equation-of-state calculations, and 505 points per wedge for the joint density of states. Core orbitals were included in a self-consistent atomic manner, except for the 4*d* states, which were treated as bands with a reduced *s-d*, 20 points/wedge basis.

The inset in Fig. 3 compared the *P-V* equation of state for fcc iodine calculated by the LMTO method (dashed curve) with the experimental data (points) and with the fit (solid curve) just described. Thermal lattice-vibrational corrections to the room-temperature data are expected to be small and have been omitted in the theoretical calculation. The theoretical results are in excellent agreement with the experimental data, and the agreement with the Vinet *et al.*[32] fit to the data continues to be quite good up to 500 GPa.

The band structure of compressed fcc iodine has been discussed some years ago.[24] The present scalar-relativistic results are in overall agreement with this early nonrelativistic work, and are shown for a volume $V=16.8$ Å^3/atom (pressure $P=108$ GPa) in Fig. 4. The three bands dropping below the Γ_{15} level are the 5*p* bands, where it is to be noted that the Δ_5 and Λ_3 branches are doubly degenerate. The 5*p* manifold is $\frac{5}{6}$ occupied as may be seen from the energy zero in the figure, which is the Fermi level. The lowest 5*d* level occurs at X_3, while hybridization between 5*d* and 4*f* states is evident from the pure-*f* Γ_2' level at the other end of the Δ_2' branch. The X_3 level remains above the Fermi energy until pressures in excess of 500 GPa, so that the 5*d* and 4*f* states remain completely empty throughout the range of interest in this paper. In analysis of the optical properties of compressed monatomic iodine, therefore, we need consider only $5p\rightarrow 5p$ and $5p\rightarrow 5d$ interband transitions. When using the notation *nl* in this way, we refer to band states according to their dominant angular-momentum

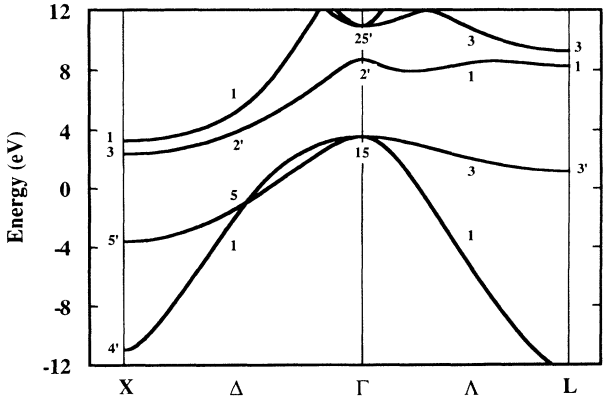

FIG. 4. Band structure of fcc iodine at 108 GPa along the [1,0,0] (Γ-Δ-*X*) and [1,1,1] (Γ-Λ-*L*) directions. The zero of energy is the Fermi level.

character, l, and atomic origin. These are hybrid Block states, however, and in the first case it is the admixture of d-like components in the predominantly p-like $5p$ states which allows interband transitions within the $5p$ manifold. In the second case, we shall no longer refer explicitly to $4f$ states, since d character is not only predominant in the upper-lying bands shown in Fig. 4 (except near Γ_2'), but also the important component for interband transitions from the $5p$ manifold.

A quantitative indication of the characteristic energy ranges for the two types of interband transitions is provided by the joint density of states $J(\hbar\omega)$, which counts all occupied-empty pairs of states having the same crystal momentum and separated by the energy $\hbar\omega$.[37] This quantity is particularly useful, since a rough approximation to the interband part of the optical conductivity $\sigma^b(\omega)$ is given by $\sigma^b(\omega) \propto J(\hbar\omega)/\omega$, on the assumption of constant dipole matrix elements.[37] Figure 5 shows $J(\hbar\omega)/\hbar\omega$ corresponding to the band structure in Fig. 4. The dashed lines in this figure resolve the total (solid line) into the separate $5p \rightarrow 5p$ and $5p \rightarrow 5d$ contributions. The $5p \rightarrow 5p$ peak seen in Fig. 5 near 1 eV arises from points in the Brillouin zone near the [1,0,0] and [1,1,1] directions, between sheets of the Fermi surface which become degenerate in the Δ_5 and Λ_3 branches, respectively, along these axes. The $5p \rightarrow 5d$ peaks between 6 and 8 eV in the figure arise from points on and about the outer halves of the [1,0,0,] axes, including the $\Delta_5 \rightarrow \Delta_2'$ and $\Delta_5 \rightarrow \Delta_1$ transitions.

The suitability of using constant matrix elements may be assessed for the case of transition metals, a particularly relevant test since these metals also have a narrow manifold of bands (nd versus the iodine $5p$) overlapping the Fermi level, with more free-electron-like states ($n+1,p$ versus the iodine $5d$) at higher energy. Comparisons of calculations with and without dipole matrix elements have been reported for rhodium and palladium,[38] and ferromagnetic iron.[39] In all cases, the constant-matrix-element approximation was seen to underestimate $\sigma^b(\omega)$ for $\hbar\omega > 6$–8 eV (dominated by $nd \rightarrow n+1,p$ transitions) relative to that at lower energies (most likely dominated by hybridization allowed $nd \rightarrow nd$ transitions) by a factor of 2–3. This approximation otherwise gave relatively faithful shapes aside from a too-low position for the first peak in $\sigma^b(\omega)$.[39,40]

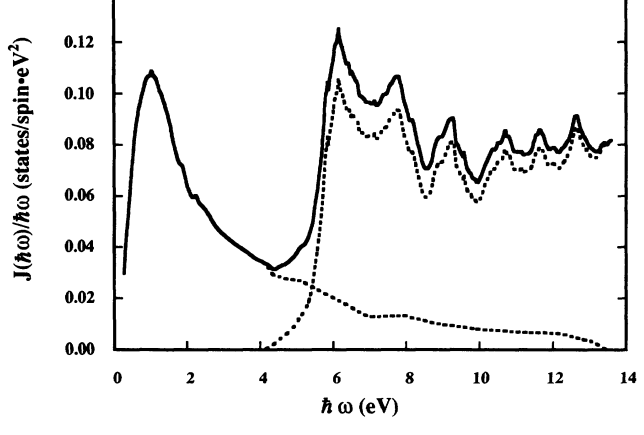

FIG. 5. The joint density of states $J(\hbar\omega)$, divided by $\hbar\omega$, corresponding to the band structure in Fig. 4. $J(\hbar\omega)/\hbar\omega$ is proportional to the interband contribution to the optical conductivity $\sigma^b(\omega)$ under the approximation of constant dipole matrix elements. The dashed curves resolve the total (solid curve) into separate $5p \rightarrow 5p$ and $5p \rightarrow 5d$ contributions.

A similar factor may be deduced for the present case of iodine within the context of the atomic-sphere approximation for the relevant squared dipole matrix element,[41] $|\langle\psi|\nabla|\psi'\rangle|^2$. If $\psi \approx c_p\phi_p + c_d\phi_d$, where ϕ_l is a muffin-tin orbital considered within a single atomic sphere, and the weights $w_l = |c_l|^2$ sum to unity for each state,[33,34] then $|\langle\psi|\nabla|\psi'\rangle|^2$ should scale roughly as $w_p w_d' + w_d w_p'$. We find $w_p w_d' + w_d w_p'$ averaged over $5p,5d$ pairs of states contributing to the 6-eV peak in Fig. 5 to be somewhat over three times larger than a similar average for the $5p,5p$ peak near 1 eV. A reasonable approximation to $\sigma^b(\omega)$ for the present case, therefore, would appear to be the sum of $5p \rightarrow 5p$ and $5p \rightarrow 5d$ contributions in Fig. 5, with the latter increased by a factor of 3. Since the additional ω^{-1} factor in the imaginary part of the dielectric function $\varepsilon_2 = 4\pi\sigma(\omega)/\omega$ emphasizes lower-energy features, and the areas (proportional to oscillator strength) of the dashed curves in the ranges 0–3 and 6–8 eV in Fig. 5 are comparable, an even simpler approximation would be to use two Lorentz oscillators with the higher-frequency oscillator having three times the oscillator strength of the lower. We calculate the reflectivity for such a simple model in the following section. Moreover, since the first peak of $\sigma^b(\omega)$ is likely to be higher than that in Fig. 5 as noted above,[40] and the local-density approximation underestimates the separation between relatively more localized and extended states, we assume somewhat larger ($\hbar\omega_0 = 1.7$ and 8 eV, respectively) positions for the frequencies of both oscillators.

Finally, it should be noted that we find the 1 and 6 eV peaks in $J(\hbar\omega)/\hbar\omega$ to be (within $\pm 4\%$) relatively independent of volume over the range 19–13.6 Å^3/atom considered here for the fcc phase, and so expect relatively little pressure dependence of the reflectivity for this phase. There is more variation in the onset of the $5p \rightarrow 5d$ transitions, seen in Fig. 5 at about 4.2 eV, and changing from about 5 to 3.3 eV over the volume interval just cited, but this will have less impact than the peak positions themselves.

REFLECTIVITY RESULTS AND MODEL ANALYSIS

A selection of the reflectivity data obtained in the present work is presented in Fig. 6, for two different samples, and for a range of pressures from 9 to 181 GPa. Due to detector sensitivity at low energies, and pressure-induced shifts in absorption by the diamond anvils at energies above about 3 eV, the relevant data to be considered lie approximately in the interval $0.5 < \hbar\omega < 3$ eV. There are two particular features of this data which are to be noted. The first is the dramatic change seen in the reflectivity below about 1 eV between the low-pressure (9 and 19 GPa) curves and those at higher pressure. This Drude-like upturn at low energies is quite familiar, and

reflects the insulator-metal transition, as has already been observed and discussed elsewhere for iodine.[17] The 19-GPa sample is in fact most likely already a metal, although with a very low plasma frequency. The second feature is the relatively large value of the reflectivity in the 1–3-eV range, which grows in size with pressure. We find, as have others,[17,27] that the combined features for iodine cannot be reproduced by a pure Drude expression for the complex dielectric function $\varepsilon(\omega)$ and that interband contributions are required. Based on a Kramers-Kronig analysis of their 29.8-GPa data, Syassen *et al.*[17] suggested an interband absorption at 1.3 eV. Natsume and co-workers simply added a real constant to the Drude expression in order to simulate the effect of interband absorptions.[27] Based on the theoretical results of the previous section, we provide a more realistic model of the dielectric function in this section, in which the absorption feature in the 1–2-eV region is attributed to hybridization-allowed $5p \rightarrow 5p$ interband excitations, a possibility which has also been acknowledged by Natsume and co-workers.[27] We suggest that the reflectivity of compressed monatomic iodine is in effect that of a *p*-like transition metal.

It should be noted, that Desgreniers, Vohra, and Ruoff[42] have recently proposed the possibility of optical transitions originating from the stressed region of the diamond-anvil cell in their analysis of high-pressure reflectivity data for oxygen. While we cannot rule out such a possibility impacting the highest-pressure reflectivity data reported here, we believe that it is unlikely to account for the non-Drude-like features seen at lower pressures, for two reasons. First, these features both in the present and earlier[17] data for iodine are fully evident near 30 GPa, far below the range above 110 GPa discussed in this regard by Desgreniers, Vohra, and Ruoff.[42] Second, the dramatic growth of reflectivity near 2 eV in the iodine experiments closely coincides in pressure with the known location of the dissociation transition in this material, suggesting an origin in the iodine sample itself.

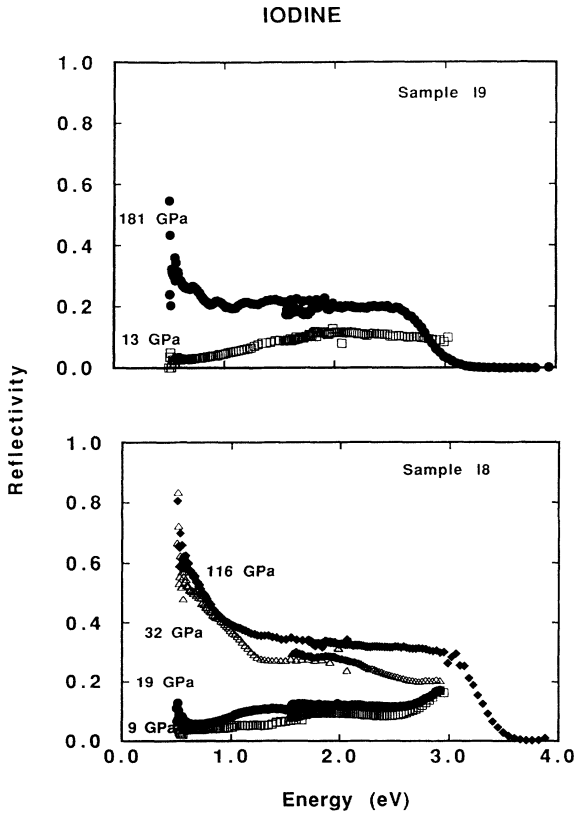

FIG. 6. Measured reflectivity of compressed iodine for two samples at six pressures as indicated. Samples at 9, 13, and 19 GPa are diatomic; those at higher pressure, monatomic. The structure at 32 GPa is bco; that at 116 and 181 GPa, fcc.

In regard to possible structural dependence of the present data, note that the 9-, 13-, and 19-GPa samples should be diatomic; while all higher-pressure data should correspond to monatomic iodine. Specifically, the sample at 32 GPa should be in the bco phase, while the 116- and 181-GPa data sets should correspond to the fcc phase of monatomic iodine. While there are significant differences in the magnitude of the present 32-GPa reflectivity and earlier data at 29.8 GPa,[17] the shapes of these two bco curves are the same. Specifically, they exhibit small or negative curvature below 1 eV, local minima and maxima at $\hbar\omega \sim 1.3$ and 2.0 eV, respectively, and a gradual drop-off above 2.0 eV. In contrast, data for the fcc phase at 57 (not shown), 116, and 181 GPa have generally positive curvature with no clear local minima or maxima in the range $0.5 < \hbar\omega < 3$ eV. We will briefly consider these shape features in our analysis.

As a model for the dielectric function in the present discussion, we shall assume the form

$$\varepsilon(\omega) = 1 - \frac{\omega_p^2}{\omega^2 + i\omega/\tau} + \sum_n \frac{\omega_p^2 f_n}{\omega_n^2 - \omega^2 - i\Gamma_n \omega} . \quad (1)$$

The first two terms give the Drude intraband contribution, where $\omega_p = (4\pi n e^2/m^*)^{1/2}$ is the plasma frequency, n and m^* are the carrier number density and effective mass, respectively, and τ is the relaxation time.[43] Note that it is rather difficult to obtain meaningful Drude parameters in cases where the interband absorption extends to very low frequencies, as for transition metals[44] and quite likely the present case as well. The third term in Eq. (1) includes the two Lorentz oscillators which we shall use to represent the $5p \rightarrow 5p$ and $5p \rightarrow 5d$ interband excitations discussed in the previous section, where ω_n and Γ_n are the oscillator frequencies and widths, respectively, and the weights f_n are essentially oscillator strengths although multiplied by m^*/m_e (m_e is the free-electron mass) compared to the usual definition.

It is instructive to consider the transition-metal analog further as a guide to our treatment of monatomic iodine. Experimental attempts have been made to determine the plasma frequency in such metals.[45] These results are generally smaller, often by a factor of 2 or more, than estimates based on valency determination of n and simple one-electron calculation[46] of m^*, suggesting that the theoretical m^* is too small by perhaps a factor of 4 (or n too large). The problem becomes more severe if one con-

siders the balance between intraband and interband contributions to the sum rule on the imaginary part ε_2 of the dielectric function.[47] In the case of Ni, for example, assuming $\hbar\omega_p = 3.0$ eV,[45] the area under $\omega\varepsilon_2(\omega)$,[44] would be consistent with $m^*/m_e > 90$ or nearly seven times the effective mass predicted from the $3d$ bandwidth.[46] Much if not all of this problem arises from having multisheet, anisotropic Fermi surfaces with mixed hole and electron character, for which the simple Drude representation is not sufficient. The Fermi surface of monatomic iodine shares these attributes. Our procedure, therefore, will be to use the transition-metal case as a guide for modifying simple theoretical estimates of the parameters in Eq. (1).

Turning to fcc iodine, our "canonical band" estimate[46] of the $5p$ effective-mass ratio m^*/m_e is 1.4 at the volume corresponding to Fig. 4.[48] Simple application of the sum rule[47] to Eq. (1) might then suggest that $\sum_n f_n = m^*/m_e - 1 = 0.4$. The transition-metal example, however, suggests that the relevant m^*/m_e here could be nearly an order of magnitude larger. In fact, we shall now show results for $f_1 = 2$ and $f_2 = 6$ keeping the ratio $f_2/f_1 = 3$ discussed previously. In addition, we take $\hbar\omega_1 = 1.7$, $\hbar\omega_2 = 8$, $\hbar\Gamma_1 = 2.3$, and $\hbar\Gamma_2 = 2$ (all in eV). The assumption of one (hole) carrier and the $m^*/m_e = 1.4$ canonical band mass suggests $\hbar\omega = 7.7$ eV at the volume corresponding to Figs. 4 and 5, which we should reduce by about a factor of 2 considering the transition-metal example. The result is close enough to the 5-eV choice of Syassen *et al.*,[17] that we adopt both of their Drude parameters, namely $\hbar\omega_p = 5$ eV and $\hbar/\tau = 0.33$ eV.

Figure 7 shows the results of calculations of the reflectivity R based on the model in Eq. (1) and the parameters just stated. Curve A shows the result obtained using just the Drude part, the first two terms. Its downward bend at the right-hand edge of the figure is an anticipation of the dramatic drop to come at the plasma frequency $\hbar\omega = 5$ eV. Curve B shows the effect of adding the lower of the two Lorentz oscillators, that simulating the $5p \rightarrow 5p$ transitions. Absorption at the frequency $\hbar\omega_1 = 1.7$ eV reduces the reflectivity over that of the free carriers, with R recovering somewhat on the high side of this absorption feature. Curve C shows the full calculation, with the second Lorentz oscillator added at $\hbar\omega_2 = 8$ eV, simulating strong $5p \rightarrow 5d$ absorption well beyond the range of the data. Nevertheless, the associated enhancement of the real part of the dielectric function, ε_1, at lower frequencies serves to reduce the plasma frequency from ω_p to an effective value roughly equal to $\omega_p(1+\varepsilon_1^{5p\rightarrow 5d})^{-1/2}$. This in turn causes the plasma-frequency-like dropoff to occur at lower energies, as seen at energies above 3 eV in curve C in the figure. Finally, curve D was calculated again with both oscillators, but with the parameters of the lower excitation changed to $\hbar\omega_1 = 1.9$ and $\hbar\Gamma_1 = 1.9$ eV.

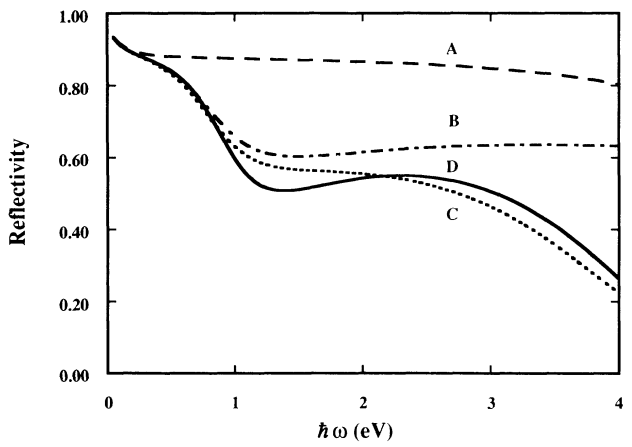

FIG. 7. Model calculations of the iodine reflectivity based on Eq. (1). Curve A includes only the Drude terms; curve B adds the lower of the two interband excitations (hybridization allowed $5p \rightarrow 5p$); while curve C is the complete calculation adding also the higher of the two interband excitations ($5p \rightarrow 5d$). Curve D is also the full calculation, with slightly adjusted parameters for the $5p \rightarrow 5p$ excitations, to simulate structural differences between the bco and fcc structures. See text.

It may be seen that curves C and D exhibit many of the essential differences seen in the fcc and bco data, respectively, in Fig. 6. There is also some theoretical justification for the parameter differences in the two cases. Since the bco phase is nearly tetragonal, we have carried out body-centered tetragonal (bct) calculations for a c/a ratio of 1.7 at the same volume as that represented for the fcc phase in Figs. 4 and 5. Due to the smaller near-neighbor distance in the bct case, we find generally broader bands, both $5p$ and $5d$, which moves the $5p \rightarrow 5p$ peak to higher energies, and also reduces the separation between the top of the $5p$ and the bottom of the $5d$ band. The former change has been reflected in the change in ω_1 for curve D, as well as a somewhat narrower width, which is also consistent with the corresponding $J(\hbar\omega)$. Both differences serve to make the ω_1 absorption feature more dramatic as is seen. The somewhat closer proximity of the $5d$ states in the tetragonal case, which has not been incorporated into the model calculations for curve D, would also depress this curve more at higher energies, in better agreement with the data.

The general features concerning the shape of the curves in Fig. 7 are in fact valid for a rather larger range of actual magnitudes for the reflectivity. Specifically, the size of R in the plateau region $\hbar\omega \sim 2$ eV is governed by the balance between the Drude and interband terms. Increased (lesser) weight in the interband terms and/or a smaller (larger) plasma frequency will lower (raise) this plateau. Clearly the dropoff to the high-energy side of this plateau also involves the combined effect of both terms in regard to the effective plasma frequency mentioned above. At low energies, it is primarily the relaxation time τ which governs the magnitude of R and the negative curvature which is very evident near $\hbar\omega = 0.5$ eV in the model calculations. A value of $\hbar/\tau$ about twice the size of the 0.33 eV used here would straighten out R in this region. It might be noted that values of $\hbar/\tau$ required to fit high-pressure reflectivity data tend on the whole to be considerably larger than found at atmospheric pressure.[45] Speculation as to the cause has included defects induced by structural transition[17] as well as plastic deformation.[42]

CONCLUSIONS

In summary, x-ray-diffraction experiments show that the fcc phase of iodine is stable from 53 to at least 276 GPa. Theoretical calculations of the equation of state for the fcc phase are in excellent agreement with the x-ray measurements to the maximum pressures (relative compression $V/V_0=0.324$). Both the present experimental reflectivity data and theoretical electronic-structure calculations suggest an absorption feature at 1–2 eV in monatomic iodine which is most likely due to hybridization-allowed $5p \rightarrow 5p$ interband transitions. Such behavior has been observed before in solid xenon compressed to a metallic state[3] but is in closer analogy to hybridization-allowed $nd \rightarrow nd$ transitions occurring in the d-like transition metals at normal conditions. Furthermore, while strong $5p \rightarrow 5d$ absorption should occur well beyond the range of the data, the effect of these interband excitations on the real part of the dielectric function is manifest in a depression of the reflectivity at the upper end of the range visible in the present experiments. Noticeable differences between data for the bco and fcc phases can be understood in terms of relatively modest changes in the respective joint densities of states.

ACKNOWLEDGMENTS

We gratefully acknowledge the technical support of Chantel Ruddle. This work was performed under the auspices of the U.S. Department of Energy by the Lawrence Livermore National Laboratory under Contract No. W-7405-ENG-48, and at the National Synchrotron Light Source, Brookhaven National Laboratory, under Contract No. DE-AC-2-76CH00016. The work performed at the Geophysical Laboratory was supported by the National Science Foundation.

[1] A. K. McMahan, Physica B **139 & 140**, 31 (1986).
[2] A. P. Jephcoat, H. K. Mao, L. W. Finger, D. E. Cox, R. J. Hemley, and C.-s. Zha, Phys. Rev. Lett. **59**, 2670 (1987).
[3] R. Reichlin, K. E. Brister, A. K. McMahan, M. Ross, S. Martin, Y. K. Vohra, and A. L. Ruoff, Phys. Rev. Lett. **62**, 669 (1989); K. A. Goettel, J. H. Eggert, and I. F. Silvera, Phys. Rev. Lett. **62**, 665 (1989).
[4] R. Reichlin, M. Ross, S. Martin, and K. Goettel, Phys. Rev. Lett. **56**, 2858 (1986).
[5] H. K. Mao, Y. Wu, R. J. Hemley, L. C. Chen, J. F. Shu, and L. W. Finger, Science **246**, 649 (1989).
[6] For a recent review, see H. K. Mao and R. J. Hemley, Am. Sci. **80**, 234 (1992).
[7] A. S. Balchan and H. G. Drickamer, J. Chem. Phys. **34**, 1948 (1961).
[8] B. M. Riggleman and H. G. Drickamer, J. Chem. Phys. **37**, 446 (1962).
[9] B. M. Riggleman and H. G. Drickamer, J. Chem. Phys. **38**, 2721 (1963).
[10] O. Shimomura, K. Takemura, Y. Fujii, S. Minomura, M. Mori, Y. Noda, and Y. Yamada, Phys. Rev. B **18**, 715 (1978).
[11] K. Takemura, Y. Fujii, S. Minomura, O. Shimomura, and Y. Fujii, Solid State Commun. **30**, 137 (1979).
[12] H. d'Amour-Sturm and W. B. Holzapfel, Physica B **139 & 140**, 328 (1986).
[13] K. Takemura, S. Minomura, O. Shimomura, and Y. Fujii, Phys. Rev. Lett. **45**, 1881 (1980).
[14] K. Takemura, S. Minomura, O. Shimomura, Y. Fujii, and J. D. Axe, Phys. Rev. B **26**, 998 (1982).
[15] Y. Fujii, K. Hase, Y. Ohishi, N. Hamaya, and A. Ondera, Solid State Commun. **59**, 85 (1986).
[16] Y. Fujii, K. Hase, N. Hamaya, Y. Ohishi, A. Ondera, G. Shimomura, and K. Takemura, Phys. Rev. Lett. **58**, 796 (1987).
[17] K. Syassen, K. Takemura, H. Tups, and A. Otto, in *Physics of Solids under Pressure,* edited by J. S. Shilling and R. N. Shelton (North-Holland, Amsterdam, 1981), p. 125.
[18] M. Pasternak, J. N. Farrell, and R. D. Taylor, Hyperfine Int. **28**, 837 (1986).
[19] M. Pasternak, J. N. Farrell, and R. D. Taylor, Solid State Commun. **61**, 409 (1987).
[20] M. Pasternak, J. N. Farrell, and R. D. Taylor, Phys. Rev. Lett. **58**, 575 (1987).
[21] O. Shimomura, K. Takemura, and K. Aoki, in *Proceedings of the Eighth Airapt International High Pressure Conference, Uppsala, Sweden 1981,* edited by C. M. Blackman, T. Johannisson, and L. Tegner (Arkitektkopia, Uppsala, 1982), p. 273.
[22] H. Fujihisa, Y. Fujii, K. Hase, Y. Ohishi, N. Hamaya, K. Tsuji, K. Takemura, O. Shimomura, H. Takahashi, and T. Nakajima, in *High Pressure Research* (Gordon and Breach, United Kingdom, 1990), Vol. 4, p. 330.
[23] A. K. McMahan, Phys. Rev. B **33**, 5344 (1986).
[24] A. K. McMahan, B. L. Hord, and M. Ross, Phys. Rev. B **15**, 726 (1977).
[25] F. Siringo, R. Pucci, and N. H. March, Phys. Rev. B **37**, 2491 (1988).
[26] N. Orita, K. Niizeki, K. Shindo, and H. Tanaka, J. Phys. Soc. Jpn. **61**, 4502 (1992).
[27] Y. Natsume and T. Suzuki, Solid State Commun. **44**, 1105 (1982); Y. Natsume, in *Solid State Physics under Pressure,* edited by S. Minomura (Terra Scientific, Tokyo, 1985), p. 43.
[28] K. Syassen and R. Sonnenshein, Rev. Sci. Instrum. **53**, 644 (1982).
[29] Y. Fei, H. K. Mao, J. Shu, and J. Hu, Phys. Chem. Miner. **18**, 416 (1992).
[30] H. K. Mao, J. Xu, and P. M. Bell, J. Geophys. Res. **91**, 4673 (1986).
[31] N. C. Holmes, J. A. Moriarty, G. R. Gathers, and W. J. Nellis, J. Appl. Phys. **56**, 2962 (1989).
[32] P. Vinet, J. Ferrante, J. R. Smith, and J. H. Rose, J. Phys. C **18**, L467 (1986).
[33] O. K. Andersen, Phys. Rev. B **12**, 3060 (1975).
[34] H. L. Skriver, *The LMTO Method* (Springer, Berlin, 1984).
[35] U. von Barth and L. Hedin, J. Phys. C **5**, 1629 (1972).
[36] E. Esposito, A. E. Carlsson, D. D. Ling, H. Ehrenreich, and C. D. Gelatt, Jr., Philos. Mag. A **41**, 251 (1980); D. Glötzel and O. K. Andersen (unpublished).
[37] M. L. Cohen and J. R. Chelikowsky, *Electronic Structure and Optical Properties of Semiconductors* (Springer-Verlag, Berlin, 1988).
[38] R. Lässer and N. V. Smith, Phys. Rev. B **25**, 806 (1982). Compare Figs. 1 and 2 to Fig. 7 in this reference.
[39] J. H. Sexton, D. W. Lynch, R. L. Benbow, and N. V. Smith, Phys. Rev. B **37**, 2879 (1988). See Fig. 4.
[40] $J(\hbar\omega)$ must approach 0 for $\hbar\omega \rightarrow 0$, since symmetry-imposed

and accidental degeneracies at the Fermi level will form a set of measure zero. In the former case, however, matrix elements between different partners (e.g., p-like x and d-like yz for Δ_5) of the same irreducible representation also vanish, suggesting a more rapid approach of $\omega\sigma^b(\omega)$ to 0. This in turn suggests that the constant-matrix-element approximation will place the lowest peak in $\sigma^b(\omega)$ at an energy which is too low.

[41]M. Alouani, J. M. Koch, and M. A. Khan, J. Phys. F **16**, 473 (1986).

[42]S. Desgreniers, Y. K. Vohra, and A. L. Ruoff, J. Phys. Chem. **94**, 1117 (1990).

[43]W. Jones and N. H. March, *Theoretical Solid State Physics* (Wiley, London, 1973), Vol. 2, Chap. 7.

[44]J. H. Weaver, C. Krafka, D. W. Lynch, and E. E. Kock, *Optical Properties of Metals* (Fachinformationszentrum, Karlsruhe, 1981).

[45]A. P. Lenham and D. M. Treherne, in *Optical Properties and Electronic Structure of Metals and Alloys,* edited by F. Abelès (North-Holland, Amsterdam, 1966), p. 196. We take $\omega_p^2 = 4\pi\sigma_{\rm op}/\tau$.

[46]O. K. Andersen and O. Jepsen, Physica B **91**, 317 (1977).

[47]See equations 7.4.7, 7.4.16, and 7.4.17 of Ref. 43.

[48]The fully hybridized $5p$ band in Fig. 4 is narrower, corresponding to $m^*/m_e \sim 1.7$; however, we use the smaller pure-p estimate to maintain consistency with the masses in Ref. 46.